Desalination and Water Treatment
www.deswater.com
doi: 10.5004/dwt.2019.24009

152 (2019) 261–267
June

Enhanced photocatalytic activity of gadolinium titanate on ofloxacin degradation after supporting on HZSM-5 zeolite

Chengzhi Jiang, Ming Han, Wenjie Zhang*

School of Environmental and Chemical Engineering, Shenyang Ligong University, Shenyang 110159, China, Tel. +86-13609880790; emails: wjzhang@aliyun.com (W. Zhang), zebra_jiang1@163.com (C. Jiang), 543687539@qq.com (M. Han)

Received 27 August 2018; Accepted 20 February 2019

ABSTRACT

Gadolinium titanate was supported on HZSM-5 zeolite by sol-gel method to prepare $Gd_2Ti_2O_7$/HZSM-5 composite. Pyrochlore structured $Gd_2Ti_2O_7$ is the solely phase of gadolinium titanate in both the unsupported $Gd_2Ti_2O_7$ and the $Gd_2Ti_2O_7$/HZSM-5, and the crystallite size of $Gd_2Ti_2O_7$ slightly decreases from 32.3 to 31.6 nm after supporting. The supported $Gd_2Ti_2O_7$ crystals do not intend to aggregate into large particles as those in the unsupported $Gd_2Ti_2O_7$. The typical functional groups in $Gd_2Ti_2O_7$, $Gd_2Ti_2O_7$/HZSM-5 and HZSM-5 are observed in Fourier transform infrared/far infrared spectra. The ofloxacin adsorption efficiency on the $Gd_2Ti_2O_7$ is 16.0%, and the efficiency is 16.8% on the supported $Gd_2Ti_2O_7$/HZSM-5, while the amount of hydroxyl radical produced on $Gd_2Ti_2O_7$/HZSM-5 under illumination is much more than the amount produced on $Gd_2Ti_2O_7$. The reaction rate constants for ofloxacin degradation are 1.05×10^{-2} and 3.52×10^{-2} min^{-1} on the pure $Gd_2Ti_2O_7$ and $Gd_2Ti_2O_7$/HZSM-5, respectively. Photocatalytic degradation efficiency increases almost linearly with rising $Gd_2Ti_2O_7$ amount when $Gd_2Ti_2O_7$ concentration is less than 400 mg L^{-1}, and the maximum photocatalytic degradation efficiency occurs in the solution containing 10 mg L^{-1} ofloxacin.

Keywords: $Gd_2Ti_2O_7$; Photocatalytic; HZSM-5; Ofloxacin; Support

1. Introduction

Antibiotics reaching the environment are harmful to the ecosystem and human health, so that such substances have to be removed from the wastewater and cannot be directly discharged into aquatic system. As it is reported that many kinds of antibiotics are observed even in the tap water, the traditional wastewater treating technique may not capable of removing all antibiotics coming from different sources. Recently, people tend to care much on reducing the hazards of antibiotics through photocatalytic oxidation technique [1–4]. Hydroxyl and $^{\cdot}O_2$ radicals can be produced during heterogeneous photocatalytic process and act as oxidative reagents to degrade many kinds of organic pollutants [5,6].

TiO_2 based materials are believed to be the most-investigated photocatalyst after half a century of intensive investigation [7–9]. At the same time, researchers have also paid great efforts on developing powerful and novel photocatalyst to fulfill the growing demand in this area. Among recently developed potential photocatalytic materials, titanates in pyrochloro and perovskite structures have aroused great attention [10,11]. As a big family of material, titanates are distinguished by the different cationic elements, and their activity also depends on preparation method, for example, hydrothermal method [12], solid state reaction [13] and sol-gel method [14].

As same as other photocatalytic materials, modification of titanate was also an effective method to enhance the photocatalytic activity, such as doping and supporting [15,16]. La/Ni was doped into $SrTiO_3$ [17] and erbium was doped into

* Corresponding author.

1944-3994/1944-3986

$CaTiO_3$ [18] to extend light absorption spectrum. Chen et al. [19] reported a new $SnS_2/La_2Ti_2O_7$ heterojunction photocatalyst for visible light activity. On the other hand, photocatalyst powder is not suitable for large-scale water treatment due to the difficulty in solid–water separation. Alternatively, photocatalyst is usually applied in the supported form, in which the selection of supporting material is the key factor [20,21]. An optimal supporting material not only acts as a support, but it can also promote the activity of photocatalyst. HZSM-5 zeolite is a porous material with the characters of large surface area and microporous structure. Guo et al. [22] and Kumari et al. [23] reported the enhanced activity of HZSM-5 supported TiO_2. In our previous work, TiO_2, $SrTiO_3$ and $La_2Ti_2O_7$ were loaded on HZSM-5 zeolite and the supported photocatalysts showed remarkable activity on photocatalytic degradation of organic substances [24–26].

In this work, $Gd_2Ti_2O_7$ was supported on HZSM-5 zeolite by sol-gel method to prepare $Gd_2Ti_2O_7$/HZSM-5 composite. The materials were characterized using X-ray powder diffraction, scanning electron microscopy, transmission electron microscopy and Fourier transform infrared/far infrared spectroscopy. Photocatalytic degradation efficiencies on both the $Gd_2Ti_2O_7$/HZSM-5 composite and the unsupported $Gd_2Ti_2O_7$ were compared to show the effects of HZSM-5 zeolite.

2. Experimental

2.1. Synthesis of $Gd_2Ti_2O_7$/HZSM-5

$Gd_2Ti_2O_7$ and $Gd_2Ti_2O_7$/HZSM-5 composite were prepared by sol-gel method, in which two precursors were prepared prior to making the sol. The precursor A was made from 1 mL tetrabutyl titanate and 8 mL ethanol, and the precursor B was made from 1.1284 g $Gd(NO_3)_3 \bullet 6H_2O$, 8 mL acetic acid and 8 mL deionized water. The n(Gd):n(Ti) ratio was 1:1 after mixing precursors A and B to obtain the final transparent sol. After 85.3 mg of HZSM-5 particles were added in the sol, the mixture was put into a 70°C water bath for sol-gel transformation. The obtained gel was dried at 110°C for 15 h, followed by 3 h calcination at 800°C. The weight percentage of $Gd_2Ti_2O_7$ in the composite was 90%.

2.2. Characterization methods

Crystal structures of the materials were analyzed by D8 Advance X-ray diffractometer with Cu Kα radiation. Surface morphologies of the materials were measured on QUANTA 250 scanning electron microscope. TEM image of the material was taken on FEI Tecnai G2 20 transmittance electron microscope. Infrared and far infrared absorption spectra were determined by Frontier FT-IR/FIR spectrometer.

2.3. Photocatalytic activity

Adsorption capacity and photocatalytic activity of $Gd_2Ti_2O_7$ and $Gd_2Ti_2O_7$/HZSM-5 composite were measured in a 100 mL quartz reactor. The mixture of 20 mg $Gd_2Ti_2O_7$ and 50 mL of 20 mg L^{-1} ofloxacin solution was stirred in the dark to measure the adsorbed percentage of ofloxacin on the material after adsorption–desorption equilibrium. The light source was a 20 W ultraviolet lamp irradiating at 253.7 nm with 2,300 μW cm^{-2}. Ofloxacin concentration in the solution was measured on 1260 high performance liquid chromatography (Agilent, USA) after removing the photocatalyst. The mobile phase was made from 1% phosphoric acid aqueous solution and acetonitrile at the volume ratio of 4:1. The concentration of ofloxacin was recorded on a UV detector after flowing out of a Zorbax Eclipse XDB-C18 (150 × 4.6 mm, 5 μm) column.

Hydroxyl radical productivity during photocatalytic process was determined in the reactor, using 20 mg $Gd_2Ti_2O_7$ and 50 mL 0.5 mmol L^{-1} terephthalic acid solution. 2-hydroxyterephthalic acid was produced after 30 min of illumination, and the solution was excited at 315 nm in LS-55 fluorescence spectrophotometer to measure the fluorescence spectrum in the wavelength between 350 and 550 nm.

3. Results and discussion

3.1. Characterization of the materials

$Gd_2Ti_2O_7$ was loaded on the surface of HZSM-5 zeolite particles by sol-gel method to prepare $Gd_2Ti_2O_7$/HZSM-5 composite, in which the weight percentage of $Gd_2Ti_2O_7$ was 90%, and the weight percentage of HZSM-5 is only 10%. Fig. 1 shows XRD patterns of $Gd_2Ti_2O_7$/HZSM-5, $Gd_2Ti_2O_7$ and HZSM-5. The diffraction pattern of pyrochlore structured $Gd_2Ti_2O_7$ is indicated by JCPDS 73-1698, which can be used to identify all diffraction peaks in the XRD pattern of the obtained pure $Gd_2Ti_2O_7$. The HZSM-5 zeolite was activated at 800°C for 3 h, so that thermal treatment of the composite at the same temperature cannot change the structure of the zeolite. However, the diffraction pattern of HZSM-5 zeolite can hardly be found in the supported $Gd_2Ti_2O_7$/HZSM-5, not only due to the small proportion of HZSM-5 in the composite but also because the HZSM-5 zeolite particles are coated with a thick $Gd_2Ti_2O_7$ layer. In this case, it seems that HZSM-5 zeolite and $Gd_2Ti_2O_7$ do not affect each other in the composite to produce any other substances besides $Gd_2Ti_2O_7$ and HZSM-5.

As can be seem from the XRD patterns of both $Gd_2Ti_2O_7$ and supported $Gd_2Ti_2O_7$/HZSM-5, well crystallized $Gd_2Ti_2O_7$

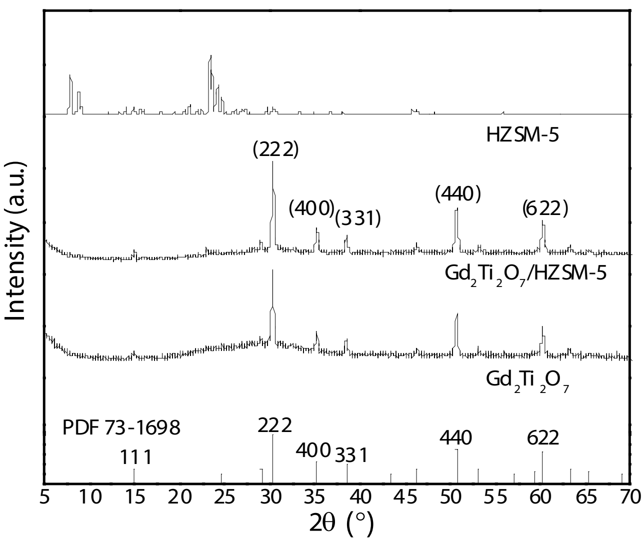

Fig. 1. XRD patterns of $Gd_2Ti_2O_7$/HZSM-5, $Gd_2Ti_2O_7$ and HZSM-5.

is produced in both the samples that are calcinated at 800°C. The preferred (222) plane of the pyrochlore $Gd_2Ti_2O_7$ was applied to calculate crystallite size using Scherrer formula. The $Gd_2Ti_2O_7$ crystallite sizes are 32.3 and 31.6 nm for the $Gd_2Ti_2O_7$ and the supported $Gd_2Ti_2O_7$/HZSM-5, respectively. Although the constrained crystal growth of photocatalyst after loading on HZSM-5 was a common observation in our previous work [24–26], the decrease in crystallite size after loading is quite small due to large $Gd_2Ti_2O_7$ content in the $Gd_2Ti_2O_7$/HZSM-5.

Fig. 2 presents the SEM images of $Gd_2Ti_2O_7$, $Gd_2Ti_2O_7$/HZSM-5 and HZSM-5, and TEM image of $Gd_2Ti_2O_7$/HZSM-5. The unsupported $Gd_2Ti_2O_7$ sample is composed of large particles in the size as large as 10 μm, and the small particles adhered on the large particle are due to grinding of the obtained sample. The typical HZSM-5 particles are in the regular shape and have smooth external surface. As shown in Fig. 2(b), the HZSM-5 particles are coated with a thick layer of $Gd_2Ti_2O_7$, whereas the shape of HZSM-5 particles cannot be distinguished in the image.

Fig. 2(d) shows the TEM image of $Gd_2Ti_2O_7$/HZSM-5 to clarify the surface morphology of the composite. $Gd_2Ti_2O_7$ crystals are coated on the surface of the HZSM-5 zeolite, and the crystal size is as same as that calculated by Scherrer formula. As a result, the surface morphology of the $Gd_2Ti_2O_7$/HZSM-5 composite is not as smooth as HZSM-5 particle. The supported $Gd_2Ti_2O_7$ crystals do not intend to aggregate into large particles that are found in the image of the unsupported $Gd_2Ti_2O_7$.

Fourier transform infrared/far infrared spectra are used to clarify the functional groups in $Gd_2Ti_2O_7$, $Gd_2Ti_2O_7$/HZSM-5 and HZSM-5, as shown in Fig. 3. The surface adsorbed hydroxyl group can be observed via its stretching vibration at 3,433 cm^{-1} and the bending vibration of water at 1,640 cm^{-1} [27]. The antisymmetric stretching vibration of Al–O–Al or Si–O–Si situates at 1,232 cm^{-1} [28], and the absorption at 796 cm^{-1} is attributed to bending vibration of Si–O–Si bond [27]. The stretching vibration of Si(Al)–O bonds in HZSM-5 zeolite at 1,060 cm^{-1} and the antisymmetric stretching vibration of the typical double pentacyclic ring at 554 cm^{-1} are the characteristics of HZSM-5 zeolite [29,30]. The absorptions of the metal-oxide groups in $Gd_2Ti_2O_7$ can be better observed in the far infrared spectra, as presented in Fig. 3(b). Both of the Ti–O bonds in octahedral TiO_6 and Si–O group in HZSM-5 have stretching vibration absorption at about 450 cm^{-1} [31]. The existence of gadolinium oxide can be proven by the stretching vibration of Gd–O at 396 cm^{-1}, the bending vibration of O–Gd–O at 295 cm^{-1}, and the stretching vibration of Gd–TiO_6 at 215 cm^{-1} [32,33].

3.2. Photocatalytic activity

Photocatalytic excitation of electrons from valence band to conduction band of photocatalyst may lead to the

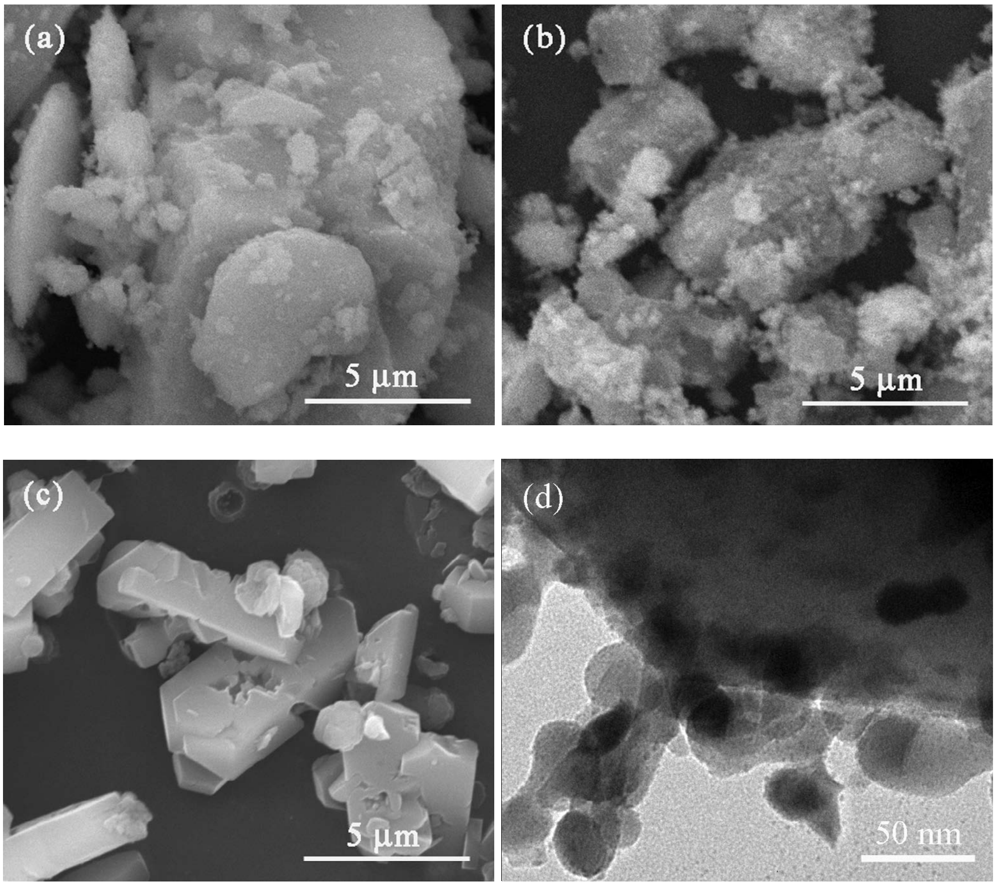

Fig. 2. SEM surface morphologies of (a) $Gd_2Ti_2O_7$, (b) $Gd_2Ti_2O_7$/HZSM-5 and (c) HZSM-5; (d) TEM image of $Gd_2Ti_2O_7$/HZSM-5.

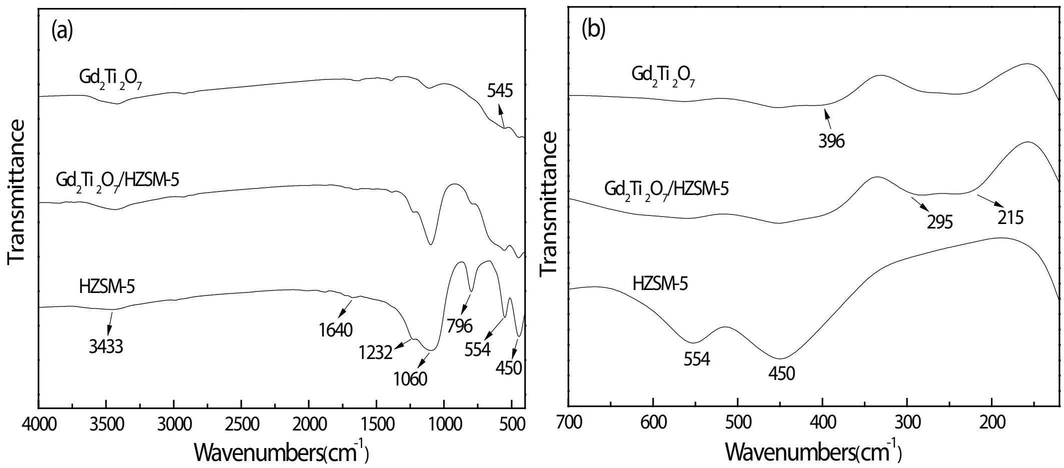

Fig. 3. (a) FT-IR and (b) Far IR spectra of $Gd_2Ti_2O_7$, $Gd_2Ti_2O_7$/HZSM-5 and HZSM-5.

generation of highly oxidative hydroxyl radical that is the major oxidative reagent in the environment. The subsequent oxidation of organic substance by hydroxyl radical is the main mechanism in photocatalytic oxidation reaction, while the reaction rate constant depends on the amount of the produced hydroxyl radical. In this work, terephthalic acid was oxidized by hydroxyl radical to produce 2-hydroxyterephthalic acid. Since 2-hydroxyterephthalic acid may emit fluorescence after excitation and the fluorescence intensity depends on the amount of 2-hydroxyterephthalic acid molecule, the amount of hydroxyl radical produced under illumination can be identified by the fluorescence intensity of the solution [34].

Fig. 4 illustrates the fluorescence spectra of 2-hydroxyterephthalic acid solution after 30 min of photocatalytic generation of hydroxyl radicals. The broad fluorescence peak centering at 426 nm can be used to compare the photocatalytic activities of $Gd_2Ti_2O_7$ and $Gd_2Ti_2O_7$/HZSM-5. Apparently, the fluorescence intensity of the solution using $Gd_2Ti_2O_7$/HZSM-5 is much stronger than the solution using $Gd_2Ti_2O_7$. This phenomenon is closely related to the enhanced photocatalytic activity of the supported $Gd_2Ti_2O_7$.

Ofloxacin molecule can be adsorbed on both $Gd_2Ti_2O_7$ and $Gd_2Ti_2O_7$/HZSM-5 in the solution. The adsorption efficiency on the pure $Gd_2Ti_2O_7$ after adsorption–desorption equilibrium is 16.0%, and the efficiency is 16.8% on the supported $Gd_2Ti_2O_7$/HZSM-5. Since the amount of $Gd_2Ti_2O_7$ is the same when using the two materials, the adsorption capacity of $Gd_2Ti_2O_7$ is almost unchanged after loading on HZSM-5. The weight percentage of $Gd_2Ti_2O_7$ in the $Gd_2Ti_2O_7$/HZSM-5 composite is 90% so that the HZSM-5 can only put very minor effect on the total adsorption capacity.

Besides adsorption of ofloxacin on the materials, photocatalytic degradation is the major pathway leading to removal of ofloxacin in the solution. Fig. 5 presents photocatalytic degradation of ofloxacin with prolonged irradiation time. As can be seen from the figure, the degradation efficiency

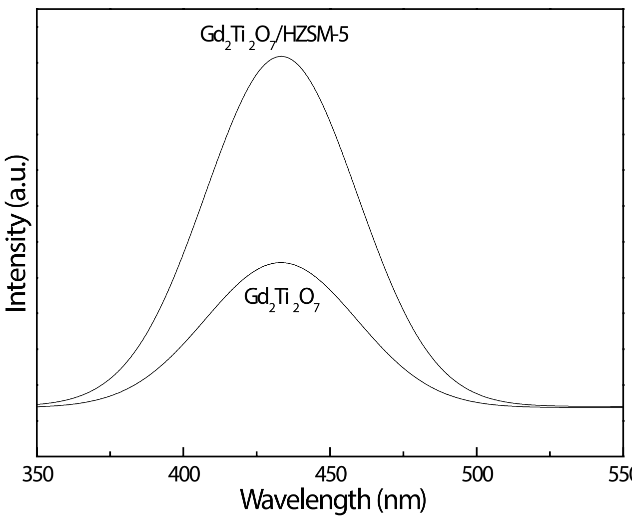

Fig. 4. Fluorescence spectra of 2-hydroxyterephthalic acid solution after 30 min of photocatalytic generation of hydroxyl radicals. 20 mg $Gd_2Ti_2O_7$ and 50 mL 0.5 mmol L^{-1} terephthalic acid solution were used.

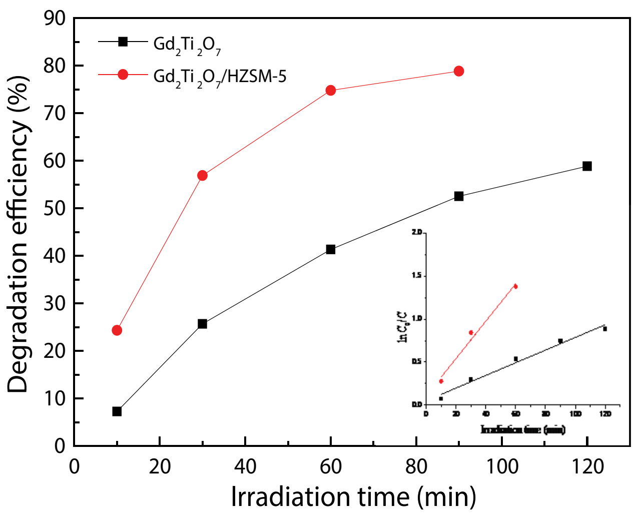

Fig. 5. Photocatalytic degradation of ofloxacin on $Gd_2Ti_2O_7$ and $Gd_2Ti_2O_7$/HZSM-5 with prolonged irradiation time. 20 mg $Gd_2Ti_2O_7$ and 50 mL of 20 mg L^{-1} ofloxacin solution were used.

continues to increase with rising irradiation time until nearly all of the ofloxacin molecules are removed from the solution when $Gd_2Ti_2O_7$/HZSM-5 is used as photocatalyst. The total removal efficiency including adsorption of ofloxacin is 95.7% after 90 min of irradiation with the existence of $Gd_2Ti_2O_7$/HZSM-5, while the total removal efficiency is only 68.1% on the $Gd_2Ti_2O_7$ after 120 min. Photocatalytic degradation of ofloxacin on the materials obeys the first order reaction law, and the reaction rate constant can be calculated via $\ln(C_0/C) = kt$ [35,36]. The reaction rate constants are 1.05×10^{-2} and 3.52×10^{-2} min^{-1} on the pure $Gd_2Ti_2O_7$ and $Gd_2Ti_2O_7$/HZSM-5, respectively.

The HZSM-5 has near no photocatalytic activity on degradation of ofloxacin in this work. The enhanced activity of $Gd_2Ti_2O_7$ after loading on HZSM-5 can only be attributed to the change in the supported $Gd_2Ti_2O_7$. As indicated before, the decrease in crystallite size after loading is quite small due to large $Gd_2Ti_2O_7$ content in the $Gd_2Ti_2O_7$/HZSM-5, and the supported $Gd_2Ti_2O_7$ crystals do not intend to aggregate into large particles that are found in the unsupported $Gd_2Ti_2O_7$. We can simply attribute the enhanced activity to the well distribution of $Gd_2Ti_2O_7$ crystals on the surface of HZSM-5 particle to reduce aggregation or agglomeration. In this case, more irradiating photons can be absorbed by the supported $Gd_2Ti_2O_7$ layer than those absorbed by the aggregated large $Gd_2Ti_2O_7$ particle, which will be absolutely beneficial to the production of hydroxyl radical and the subsequent degradation of ofloxacin.

Fig. 6 shows adsorption and photocatalytic degradation of ofloxacin as a factor of $Gd_2Ti_2O_7$/HZSM-5 amount in the solution. Ofloxacin removal efficiency by both adsorption and photocatalytic degradation is affected by the variation of photocatalyst amount when ofloxacin solution concentration is maintained at 20 mg L^{-1}. The adsorption of ofloxacin on the material continuously increases with rising $Gd_2Ti_2O_7$ amount. On the other hand, photocatalytic degradation efficiency increases almost linearly with rising $Gd_2Ti_2O_7$ amount when $Gd_2Ti_2O_7$ concentration is less than 400 mg L^{-1}, and subsequently, photocatalytic degradation efficiency nearly does not change with increasing $Gd_2Ti_2O_7$ concentration. Excessive $Gd_2Ti_2O_7$/HZSM-5 in the solution may result in agglomeration of the supported particles [37,38]. 400 mg L^{-1} of $Gd_2Ti_2O_7$ seems to be the optimal concentration in 20 mg L^{-1} ofloxacin solution, and this concentration is adopted in this work.

Since initial ofloxacin concentration varies in wastewater, it is meaningful to study the effects of ofloxacin concentration on the removal efficiency. Fig. 7 presents adsorption and 30 min of photocatalytic degradation of ofloxacin as a factor of initial ofloxacin concentration in the solution containing $Gd_2Ti_2O_7$/HZSM-5. The ofloxacin adsorption efficiency decreases with rising ofloxacin concentration, which is due to the limited adsorption capacity of the material. However, the change in photocatalytic degradation efficiency shows a different trend.

When ofloxacin concentration is not more than 10 mg L^{-1}, the degradation efficiency almost increases linearly with rising ofloxacin concentration. Since the amount of $Gd_2Ti_2O_7$/HZSM-5 is unchanged in this experiment, the amount of oxidative reagents such as hydroxyl radical is the same in spite of the variation of ofloxacin concentration. However, the ofloxacin molecules have to be adsorbed on the surface of $Gd_2Ti_2O_7$/HZSM-5 before they can react with the photogenerated oxidative reagents. The continuous adsorption rate of ofloxacin molecules from the solution at low concentration cannot be as fast as that in the solution at high concentration due to low collision frequency for photocatalyst particles and ofloxacin molecules.

A well-known situation is that the photogenerated electrons and holes, as well as the subsequently produced hydroxyl radicals, have very short lifetime. They can adequately take part in the degradation reaction if sufficient ofloxacin molecules are in the solution [39,40]. As a result,

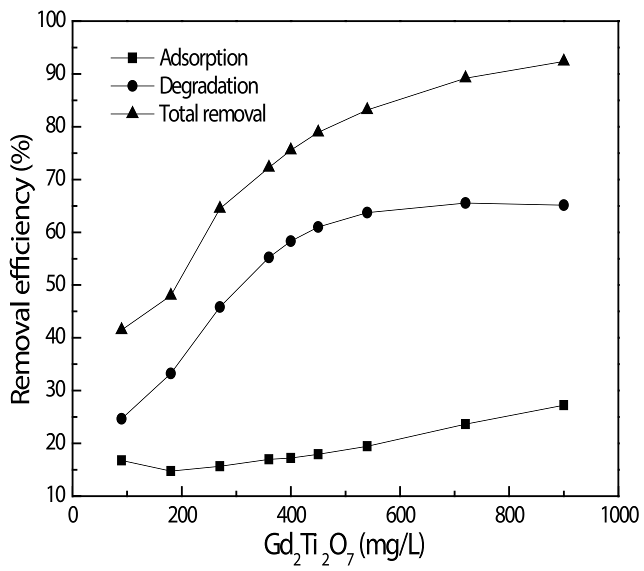

Fig. 6. Adsorption and photocatalytic degradation of ofloxacin as a factor of $Gd_2Ti_2O_7$/HZSM-5 amount in 50 mL of 20 mg L^{-1} ofloxacin solution.

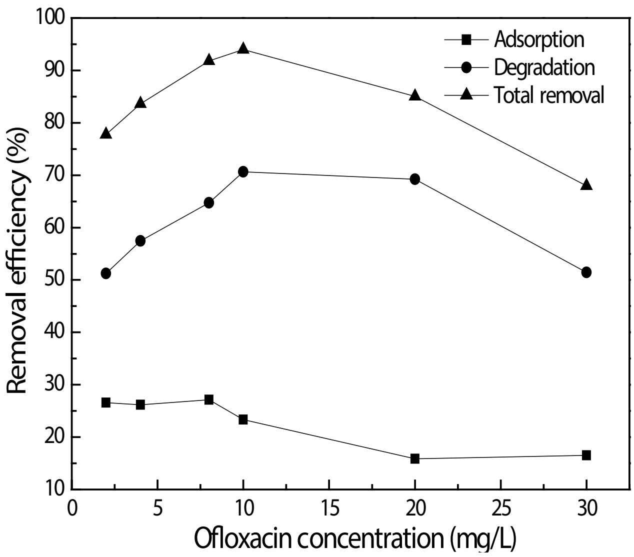

Fig. 7. Adsorption and photocatalytic degradation of ofloxacin on $Gd_2Ti_2O_7$/HZSM-5 as a factor of initial ofloxacin concentration. The irradiation time was 30 min, and 20 mg $Gd_2Ti_2O_7$ was used.

the maximum photocatalytic degradation efficiency occurs in the solution containing 10 mg L^{-1} ofloxacin. On the other hand, when ofloxacin concentration is more than 10 mg L^{-1}, the degradation efficiency declines with increasing ofloxacin concentration since the amount of reactant exceeds the capacity of the photocatalyst.

4. Conclusions

$Gd_2Ti_2O_7$/HZSM-5 composites were prepared to investigate the effects of supporting on the properties of the $Gd_2Ti_2O_7$ photocatalyst. The crystallite size of the pyrochlore $Gd_2Ti_2O_7$ is almost unchanged after loading. The HZSM-5 particles are coated with a thick layer of $Gd_2Ti_2O_7$ and the aggregation of $Gd_2Ti_2O_7$ crystals is inhibited. The absorptions of the metal-oxide groups in $Gd_2Ti_2O_7$ can be observed in the infrared spectra. Hydroxyl radical productivity in the solution using $Gd_2Ti_2O_7$/HZSM-5 is much larger than that using $Gd_2Ti_2O_7$. The total removal efficiency including adsorption of ofloxacin is 95.7% after 90 min of irradiation with the existence of $Gd_2Ti_2O_7$/HZSM-5, while the total removal efficiency is only 68.1% on the $Gd_2Ti_2O_7$ after 120 min. 400 mg L^{-1} of $Gd_2Ti_2O_7$ seems to be the optimal photocatalyst concentration in 20 mg L^{-1} ofloxacin solution.

Acknowledgments

This work was supported by Scientific Research Fund of Liaoning Provincial Education Department, China (No. LG201604), and the Natural Science Foundation of Liaoning Province, China (No. 201602644).

References

[1] N. Arabpour, A. Nezamzadeh-Ejhieh, Modification of clinoptilolite nano-particles with iron oxide: increased composite catalytic activity for photodegradation of cotrimaxazole in aqueous suspension, Mater. Sci. Semicond. Process., 31 (2015) 684–692.
[2] W.J. Zhang, J. Yang, C.G. Li, Role of thermal treatment on sol-gel preparation of porous cerium titanate: characterization and photocatalytic degradation of ofloxacin, Mater. Sci. Semicond. Process., 85 (2018) 33–39.
[3] W.J. Zhang, Y.J. Tao, C.G. Li, Effects of PEG4000 template on sol-gel synthesis of porous cerium titanate photocatalyst, Solid State Sci., 78 (2018) 16–21.
[4] H. Derikvandi, A. Nezamzadeh-Ejhieh, Synergistic effect of p-n heterojunction, supporting and zeolite nanoparticles in enhanced photocatalytic activity of NiO and SnO_2, J. Colloid Interface Sci., 490 (2017) 314–327.
[5] H. Derikvandi, A. Nezamzadeh-Ejhieh, Designing of experiments for evaluating the interactions of influencing factors on the photocatalytic activity of NiS and SnS_2: focus on coupling, supporting and nanoparticles, J. Colloid Interface Sci., 490 (2017) 628–641.
[6] P. Mohammadyari, A. Nezamzadeh-Ejhieh, Supporting of mixed ZnS–NiS semiconductors onto clinoptilolite nano-particles to improve its activity in photodegradation of 2-nitrotoluene, RSC Adv., 5 (2015) 75300–75310.
[7] H. Zabihi-Mobarakeh, A. Nezamzadeh-Ejhieh, Application of supported TiO_2 onto Iranian clinoptilolite nanoparticles in the photodegradation of mixture of aniline and 2, 4-dinitroaniline aqueous solution, J. Ind. Eng. Chem., 26 (2015) 315–321.
[8] W.J. Zhang, Y.X. Liu, X.B. Pei, X.J. Chen, Effects of indium doping on properties of xIn-0.1%Gd-TiO_2 photocatalyst synthesized by sol-gel method, J. Phys. Chem. Solids, 104 (2017) 45–51.
[9] W.J. Zhang, F.F. Bi, Y. Yu, H.B. He, Phosphoric acid treating of ZSM-5 zeolite for the enhanced photocatalytic activity of TiO_2/HZSM-5, J. Mol. Catal. A: Chem., 372 (2013) 6–12.
[10] Z. Chen, H. Jiang, W. Jin, C. Shi, Enhanced photocatalytic performance over $Bi_4Ti_3O_{12}$ nanosheets with controllable size and exposed {001} facets for Rhodamine B degradation, Appl. Catal., B, 180 (2016) 698–706.
[11] W.J. Zhang, Y.J. Tao, C.G. Li, Sol-gel synthesis and characterization of $Gd_2Ti_2O_7$/SiO_2 photocatalyst for ofloxacin decomposition, Mater. Res. Bull., 105 (2018) 55–62.
[12] W.M. Hou, Y. Ku, Synthesis and characterization of $La_2Ti_2O_7$ employed for photocatalytic degradation of reactive red 22 dyestuff in aqueous solution, J. Alloys Compd., 509 (2011) 5913–5918.
[13] K. Onozuka, Y. Kawakami, H. Imai, T. Yokoi, T. Tatsumi, J.N. Kondo, Perovskite-type $La_2Ti_2O_7$ mesoporous photocatalyst, J. Solid State Chem., 192 (2012) 87–92.
[14] L.L. Zhang, H. Zhong, W.G. Zhang, L. Lu, X.J. Yang, X. Wang, Fabrication of $Dy_2Ti_2O_7$ nanocrystalline at 700°C and its photocatalytic activity, J. Alloys Compd., 463 (2008) 466–470.
[15] J. Esmaili-Hafshejani, A. Nezamzadeh-Ejhieh, Increased photocatalytic activity of Zn(II)/Cu(II) oxides and sulfides by coupling and supporting them onto clinoptilolite nanoparticles in the degradation of benzophenone aqueous solution, J. Hazard. Mater., 316 (2016) 194–203.
[16] H. Derikvandi, A. Nezamzadeh-Ejhieh, A comprehensive study on enhancement and optimization of photocatalytic activity of ZnS and SnS_2: Response surface methodology (RSM), n-n heterojunction, supporting and nanoparticles study, J. Photochem. Photobiol., A, 348 (2017) 68–78.
[17] F. Li, K. Yu, L. Lou, Z. Su, S. Liu, Theoretical and experimental study of La/Ni co-doped $SrTiO_3$ photocatalyst, Mater. Sci. Eng., B, 172 (2010) 136–141.
[18] L.M. Lozano-Sánchez, S. Obregón, L.A. Díaz-Torres, S. Lee, V. Rodríguez-González, Visible and near-infrared light-driven photocatalytic activity of erbium-doped $CaTiO_3$ system, J. Mol. Catal. A: Chem., 410 (2015) 19–25.
[19] J. Chen, S. Liu, L. Zhang, N. Chen, New SnS_2/$La_2Ti_2O_7$ heterojunction photocatalyst with enhanced visible-light activity, Mater. Lett., 150 (2015) 44–47.
[20] A. Nezamzadeh-Ejhieh, M. Bahrami, Investigation of the photocatalytic activity of supported ZnO-TiO_2 on clinoptilolite nano-particles towards photodegradation of wastewater-contained phenol, Desal. Wat. Treat., 55 (2015) 1096–1104.
[21] H. Derikvandi, A. Nezamzadeh-Ejhieh, Increased photocatalytic activity of NiO and ZnO in photodegradation of a model drug aqueous solution: Effect of coupling, supporting, particles size and calcination temperature, J. Hazard. Mater., 321 (2017) 629–638.
[22] P. Guo, X.S. Wang, H.C. Guo, TiO_2/Na-HZSM-5 nano-composite photocatalyst: Reversible adsorption by acid sites promotes photocatalytic decomposition of methyl orange, Appl. Catal., B, 90 (2009) 677–687.
[23] V.D. Kumari, M. Subrahmanyam, K.V. Subba Rao, A. Ratnamala, M. Noorjahan, K. Tanaka, An easy and efficient use of TiO_2 supported HZSM-5 and TiO_2+HZSM-5 zeolite combinate in the photodegradation of aqueous phenol and *p*-chlorophenol, Appl. Catal., A, 234 (2002) 155–165.
[24] W.J. Zhang, Z. Ma, K.X. Li, L.L. Yang, H. Li, H.B. He, Sol-gel Synthesis of Nano-sized TiO_2 Supported on HZSM-5, Curr. Nanosci., 12 (2016) 514–519.
[25] W. Zhang, L. Du, F. Bi, H. He, A novel $SrTiO_3$/HZSM-5 photocatalyst prepared by sol–gel method, Mater. Lett., 157 (2015) 103–105.
[26] W.J. Zhang, Z. Ma, L. Du, L.L. Yang, X.J. Chen, H.B. He, Effects of calcination temperature on characterization and photocatalytic activity of $La_2Ti_2O_7$ supported on HZSM-5 zeolite, J. Alloys Compd., 695 (2017) 3541–3546.
[27] W.J. Zhang, K.L. Wang, Y. Yu, H.B. He, TiO_2/HZSM-5 nano-composite photocatalyst: HCl treatment of NaZSM-5 promotes photocatalytic degradation of methyl orange, Chem. Eng. J., 163 (2010) 62–67.
[28] W.G. Guo, Q. Xin, H. Zhang, J. Liang, Structure analysis of ZSM-5 type zeolite by infrared spectroscopy, Chin. J. Catal., 2 (1981) 36–41.
[29] X. Li, B. Li, J. Xu, Q. Wang, X.M. Pang, X.H. Gao, Z.Y. Zhou, J.R. Piao, Synthesis and characterization of Ln-ZSM-5/MCM-41

(Ln = La, Ce) by using kaolin as raw material, Appl. Clay Sci., 50 (2010) 81–86.
[30] A. Nezamzadeh-Ejhieh, A. Shirzadi, Enhancement of the photocatalytic activity of ferrous oxide by doping onto the nano-clinoptilolite particles towards photodegradation of tetracycline, Chemosphere, 107 (2014) 136–144.
[31] L. Zhang, Z. Xing, H. Zhang, Z. Li, X.Y. Wu, X.D. Zhang, Y. Zhang, W. Zhou, High thermostable ordered mesoporous SiO_2–TiO_2 coated circulating-bed biofilm reactor for unpredictable photocatalytic and biocatalytic performance, Appl. Catal., B, 180 (2016) 521–529.
[32] A. Garbout, N. Kallelkchaou, M. Férid, Relationship between the structural characteristics and photoluminescent properties of $LnEuTi_2O_7$ (Ln=Gd and Y) pyrochlores, J. Lumin., 169 (2016) 359–366.
[33] A. Garbout, I.B. Taazayet-Belgacem, M. Férid, Structural, FT-IR, XRD and Raman scattering of new rare-earth-titanate pyrochlore-type oxides $LnEuTi_2O_7$ (Ln = Gd, Dy), J. Alloys Compd., 573 (2013) 43–52.
[34] Y. Hu, Q.Y. Fang, J.Z. Zhou, D.P. Zhan, K. Shi, Z.Q. Tian, Z.W. Tian, Factors influencing hydroxyl radical formation in a photo-induced confined etching system, Acta Phys. Chim. Sin., 29 (2013) 2392–2398.
[35] A. Nezamzadeh-Ejhieh, S. Hushmandrad, Solar photo-decolorization of methylene blue by CuO/X zeolite as a heterogeneous catalyst, Appl. Catal., A, 388 (2010) 149–159.
[36] Z. Shams-Ghahfarokhi, A. Nezamzadeh-Ejhieh, As-synthesized ZSM-5 zeolite as a suitable support for increasing the photoactivity of semiconductors in a typical photodegradation process, Mater. Sci. Semicond. Process., 39 (2015) 265–275.
[37] Z.A. Mirian, A. Nezamzadeh-Ejhieh, Removal of phenol content of an industrial wastewater via a heterogeneous photodegradation process using supported FeO onto nanoparticles of Iranian clinoptilolite, Desal. Wat. Treat., 57 (2016) 16483–16494.
[38] S. Mousavi-Mortazavi, A. Nezamzadeh-Ejhieh, Supported iron oxide onto an Iranian clinoptilolite as a heterogeneous catalyst for photodegradation of furfural in a wastewater sample, Desal. Wat. Treat., 57 (2016) 10802–10814.
[39] A. Nezamzadeh-Ejhieh, M. Khorsandi, Heterogeneous photodecolorization of Eriochrome Black T using Ni/P zeolite catalyst, Desalination, 262 (2010) 79–85.
[40] A. Nezamzadeh-Ejhieh, M. Khorsandi, Photodecolorization of Eriochrome Black T using NiS-P zeolite as a heterogeneous catalyst, J. Hazard. Mater., 176 (2010) 629–637.